bradscholars

Fibrillation of chain branched poly (lactic acid) with improved blood compatibility and bionic structure

Item Type	Article
Authors	Li, Z.;Zhao, X.;Ye, L.;Coates, Philip D.;Caton-Rose, Philip D.;Martyn, Michael T.
Citation	Li Z, Zhao X, Ye L, Coates PD, Caton-Rose PD and Martyn MT (2015) Fibrillation of Chain branched Poly (lactic acid) with Improved Blood Compatibility and Bionic Structure. Chemical Engineering Journal. 279: 767-776.
DOI	https://doi.org/10.1016/j.cej.2015.05.082
Rights	© 2015 Elsevier B.V. Full-text reproduced in accordance with the publisher's self-archiving policy. This manuscript version is made available under the CC-BY-NC-ND 4.0 license http://creativecommons.org/licenses/by-nc-nd/4.0/
Download date	2025-04-24 23:28:08
Link to Item	http://hdl.handle.net/10454/8030

UNIVERSITY of BRADFORD

Library

The University of Bradford Institutional Repository

http://bradscholars.brad.ac.uk

This work is made available online in accordance with publisher policies. Please refer to the repository record for this item and our Policy Document available from the repository home page for further information.

To see the final version of this work please visit the publisher's website. Access to the published online version may require a subscription.

Link to publisher's version: *http://dx.doi.org/10.1016/j.cej.2015.05.082*

Citation: Li Z, Zhao X, Ye L, Coates PD, Caton-Rose F and Martyn MT (2015) Fibrillation of Chain branched Poly (lactic acid) with Improved Blood Compatibility and Bionic Structure. Chemical Engineering Journal. 279: 767-776.

Copyright statement: © 2015 Elsevier B.V. Full-text reproduced in accordance with the publisher's self-archiving policy.

This manuscript version is made available under the CC-BY-NC-ND 4.0 license
http://creativecommons.org/licenses/by-nc-nd/4.0/

Fibrillation of Chain branched Poly (lactic acid) with Improved Blood Compatibility and Bionic Structure

[1]Zhengqiu Li, [1]Xiaowen Zhao*, [1]Lin Ye, [2]Phil Coates, [2]Fin Caton-Rose, [2]Michasel Martyn

1. State Key Laboratory of Polymer Materials Engineering of China, Polymer Research Institute of Sichuan University, Chengdu, China

2. School of Engineering, Design and Technology, University of Bradford, Bradford, U.K.

*Corresponding author. Tel.: 862885408802; Fax: 862885402465. E-mail address: zhaoxiaowenscu@126.com

Abstract: Highly-oriented poly (lactic acid) (PLA) with bionic fibrillar structure and micro-grooves was fabricated through solid hot drawing technology for further improving the mechanical properties and blood biocompatibility of PLA as blood-contacting medical devices. In order to enhance the melt strength and thus obtain high orientation degree, PLA was first chain branched with pentaerythritol polyglycidyl ether (PGE). The branching degree as high as 12.69 mol% can be obtained at 0.5wt% PGE content. The complex viscosity, elastic and viscous modulus for chain branched PLA were improved resulting from the enhancement of molecular entanglement, and consequently higher draw ratio can be achieved during the subsequent hot stretching. The stress-induced crystallization of PLA occurred during stretching, and the crystal structure of the oriented PLA can be attributed to the α' crystalline form. The tensile strength and modulus of PLA were improved dramatically by drawing. Chain branching and orientation could significantly enhance the blood compatibility of PLA by prolonging clotting time and decreasing hemolysis ratio, protein adsorption and platelet activation. Fibrous structure as well as micro-grooves can be observed for the oriented PLA which were similar to intimal layer of blood vessel, and this bionic structure was considered to be beneficial to decrease the activation and/or adhesion of platelets.

Keywords: Poly (lactic acid) (PLA); chain branching; fibrillation; mechanical properties; blood compatibility; bionic character

Introduction

Poly (lactic acid) (PLA, -[CH(CH_3)COO]$_n$-) is a linear aliphatic thermoplastic polyester which is produced from lactic acid by converting sugar or starch obtained from renewable sources (e.g., corn, wheat, or rice) [1]. PLA has been considered to be a good candidate for biomedical materials due to its favorable physical properties, ease of handling and processing, and it's biodegradable and biocompatible nature, which have been approved by the Food and Drug Administration (FDA) for numerous clinical applications, such as sutures, bone plates, abdominal mesh, and extended-release pharmaceuticals [2~4].

For all implanted biomaterials and biodevices, the central characteristics are their biofunctionality and biocompatibility [5~6]. Biofunctionality is related to the material physical and chemical characteristics which allow a device to perform a required function. Mechanical characteristics after implantation is an important part of biofunctionality, for example, the flexibility or rigidity and mechanical strength must fulfill the purposes for multiple practices relating to biological preference. Biocompatibility refers broadly to safety and lack of adverse interactions of the implant over its intended lifetime in the body, and it is more difficult to achieve. Since blood is the first body fluid that contacts any implant, blood compatibility is proved one of the most important biocompatible properties to ensure the security of clinical practice.

Although extensive efforts have been devoted to improve the mechanical properties of PLA by copolymerization with other monomers or blending with other materials, the strength and modulus of PLA are still not sufficient for implant fixation. On the other hand, to improve the blood compatibility of PLA, surface coating and surface modification, such as chemical modification with drugs and endothelial cell seeding, are the most general approaches. However, these methods still have some problems. Surface chemical modification requires rather complex experimental procedures and involves high costs, and long term stability is

additional aspect requiring improvement [7]. Endothelial cell seeding has the potential to provide effective surface modification. However, the adhesion and proliferation of endothelial cells on artificial surfaces are very complex phenomena, so the formation of these cell layers is a very slow process [8].

Molecular orientation in polymers greatly improves their mechanical and physical properties compared to isotropic materials [9]. Solid phase hot drawing is one of the methods of molecular orientation in the solid state of polymers [10]. Through such technology, first of all, PLLA with sufficient strength could be prepared to meet the requirement of desirable physical properties for biomedical use [11~12]. Meanwhile, the surface properties of PLA may be influenced by processing and thus affect the interaction with the biological elements of the organism. Grijpma et al. reported that oriented poly (D,L-lactide) could be obtained by drawing injection molded specimens at temperatures below the glass transition temperature of the polymer [13]. High mechanical properties, with tensile strength of 73 MPa, elongation at break of 48% and the charpy impact strength of 35 KJ/m^2 were achieved. Yang et al. reported orientation-structured microtubules of PLA prepared by phase separation of the polymer solution through the process of freeze-drying [14]. Wong et al. described uni-axial stretching of PLA carried out on a universal Instron Testing Machine [15]. However, compared with some reported oriented polymers such as polyethylene, polypropylene and so on, it is very difficult to be ultra-drawn for PLA due to its low viscosity and poor melt strength. Moreover, the effect of orientation on the blood compatibility of PLA has not been studied.

In this work, PLA was chain branched with pentaerythritol polyglycidyl ether (PGE) through reactive processing in order to enhance the molecular entanglement and melt strength of PLA. And then highly oriented PLA with fibrillar structure as well as submicrometer structures can be expected to be formed through solid hot drawing technology. The structure

and properties of the oriented PLA were studied, and its bionic character as well as anti-coagulation mechanism were tried to be explored.

2. Experimental Section

2.1 Materials

Poly (lactic acid) (PLA) (NatureWorks® PLA Polymer 3052D) was supplied from Nature Works in pellet form. The molecular weight ($\overline{M_w}$) was about 1×10^5. Pentaerythritol polyglycidyl ether (PGE) (AR) was obtained from Energy Chemical Co. Ltd., China.

2.2 Preparation of the highly oriented PLA

Chain branched PLA

After dried at 70°C for 5hrs in a vacuum oven, PLA was mixed with varying PGE contents (0.1% , 0.3%, 0.5%, 0.7%, 1%, 3%, 5% by weight based on PLA, respectively) in a Haake internal melt mixer (Rheocord 90, Germany) at 170°C, and then the product was cut into small granules. Dumbbell shaped specimens were molded by micro-injection molding machine at 170°C.

Highly oriented PLA

The oriented samples of PLA and chain branched PLA were prepared by being heated and mechanically drawn. After the desired draw ratio was obtained, the sample was cooled down to room temperature, and then the load was released.

2.3 Measurements

^{13}C NMR spectra

^{13}C NMR measurements of PLA were performed with Advance Bruker 600 NMR spectrometer (Bruker Co, Germany) at 600 MHz at room temperature, using $CDCl_3$ as solvent.

Dynamic Rheological Analysis

Dynamic rheological measurement was performed on an AR 1500ex dynamic stress rheometer (TA Instruments, USA). The samples were compression molded into the disk of 25 mm in diameter and around 1 mm in thickness. The measurement was run with a 25 mm-diameter parallel plate geometry and a 1.0-mm sample gap. The dynamic viscoelastic properties were determined with frequencies from 0.01 to 100 Hz at 170°C, using 1% strain (selected after strain sweep tests) value determined with a stress sweep to keep within the linear viscoelastic region. Specimens were placed between the preheated plates at the experimental temperature and were allowed to equilibrate before each run.

Mechanical properties

The mechanical properties of PLA samples were measured with a 4302 material testing machine (Instron Co, USA) according to ISO527/1-1993 (E). The test speed was 50 mm/min, and the sample length between benchmarks was 25 mm.

Two-dimensional Wide-angle X-ray diffraction analysis (2D-WAXD)

Wide-angle X-ray diffraction (WAXD) analysis was conducted at the ambient temperature using a D8 Discover two-dimensional wide angle X-ray diffractometer (2d-WAXD) (Bruker AXS Co, Germany). The sampling time of 2d-WAXD measurements was 180 s using an Eulerian 1/4 cradle HI-STAR (2D-Detector) detector, with a wavelength of 0.154 nm monochromated X-ray obtained from Cu (Kα) radiation.

Scanning electron microscope analysis (SEM)

The fractured surface morphology analysis of the samples was performed with JEOL JSM-5900LV scanning electron microscope (SEM, JEOL Co, Japan) with an acceleration voltage of 20 kV. The samples were sputter-coated with gold for 2~3 min.

AFM observation

Atomic force microscopy (AFM) was used to determine the topographic change of the surface at different draw ratios. The AFM observations were performed on a Dimension 3100

Nanoscope IV equipped with Silicon TESP cantilevers (Shimadzu SPM-9600, Japan) in a non-contact (taping) mode.

Protein adsorption

Protein adsorption experiments were carried out with bovine serum albumin (BSA) and bovine serum fibrinogen (BFG) solutions under the static condition. Firstly, the samples with an area of 0.4 cm×0.5 cm was immersed in a phosphate buffer solution (PBS), containing BSA or BFG with the concentration of 1 mg/mL, and incubated at 37°C for 1 h; then the samples was rinsed slightly with PBS solution and double distilled water. Then the samples was placed in a washing solution (2% sodium dodecyl sulfate (SDS) and 0.05 M NaOH) at 37°C, and shaken for 2 h to remove the adsorbed protein. The protein concentration in the washing solution was determined by using the Micro BCATM Protein Assay Reagent Kit (PIERCE), and then the adsorbed protein amount was calculated.

Platelet adhesion measurement

To test the platelet adhesion, samples were incubated with the platelet rich plasma (PRP) for 1 h at 37°C under static conditions. After 1 h incubation, the samples were rinsed carefully three times with phosphate-buffered saline (PBS, pH=7.3) buffer. The adherent platelets were fixed using 2.5% glutaraldehyde in PBS for at least 1 h, dehydrated in a graded series (50%, 60%, 70%, 80%, 90%, 95%, and 100%, v/v) of ethanol, and dried under vacuum at -50°C overnight. The samples were then sputter coated with a thin layer of gold and observed using a scanning electron microscopy (JEOL JSM-5900LV).

Hemolysis analysis

Hemolytic activity was assessed by determining hemoglobin release under static conditions using the two phase hemolysis test (according to ASTM F 756-00). Blood testing solution was prepared by using 4 mL fresh blood with an acid citrate dextrose anticoagulant (ACD medium) and was diluted with 5 ml of physiological saline. In the first phase, each

sample was incubated in 10 ml neat saline for 30 min at 37°C. Then, diluted fresh blood (0.2 mL) was added and incubation went on for another 60 min in a shaker at the constant temperature of 37°C. Positive and negative controls were produced by adding 0.2 mL of diluted fresh blood to 10 ml of purified water and saline, respectively. After incubation, samples were centrifuged at 2500 r/min for 5 min. Optical density of the supernatant was measured at 545 nm by a spectrophotometer. The hemolysis ratio was calculated according to Eq.1:

$$Z=100\%*(D_t-D_{nc})/(D_{pc}-D_{nc}) \qquad (1)$$

Where Z represented the hemolysis ratio, D_t represented the absorptance of test samples, D_{nc} and D_{pc} represented the negative samples and positive samples, respectively (ASTM F 756-00).

Clotting time (APTT and TT)

Activated partial thromboplastin time (APTT) and thrombin time (TT) were measured by an automated blood coagulation analyzer CA-50 (Sysmex Corporation, Kobe, Japan), and the test method was described as follows: fresh blood was collected using vacuum tubes, containing sodium citrate as an anticoagulant (anticoagulant to blood ratio, 1:9, v/v). The platelet-poor plasma (PPP) was obtained after centrifuging at 4000 rpm for 15 min. Synchronously, the samples (0.4 cm×0.5 cm) were immersed in PBS (0.2 mL, pH = 7.4) for 1 h. Then the PBS was removed and 0.1 mL of fresh PPP was introduced. After incubating at 37°C for 30 min, 50μL of the incubated PPP was added into the test cup, followed by the addition of 50μL of APTT agent (incubated 10 min before use) and incubation at 37°C for 3 min. Thereafter, 50μL of 0.025 M $CaCl_2$ solution was added, and then the APTT was measured. For the TT test, 50μL of TT agent was added into the test cup (containing 50μL of the incubated PPP) after 10 min incubating, and then the TT was measured. At least three

measurements were averaged to get a reliable value, and the results were analyzed by statistical method.

Statistical analysis

The quantitative results were obtained from triplicate samples and the data was expressed as mean ± SD (n = 3 or 5). Statistical analysis was performed using one-way analysis of variance, followed by post hoc Student's t-test. A value of $p < 0.05$ was considered to be statistically significant.

3. Results and Discussion

3.1 Characterization of chain branched PLA

PLA was chain branched by tetra-functional epoxides PGE through reactive processing. Polyester/epoxide reactions have been widely investigated in the past [16~19], which showed that epoxide groups can react with both terminal carboxyl and terminal hydroxyl groups of polyester. However, according to the literature, the reactivity of epoxide with carboxyl group precedes hydroxyl group. [20~22] Therefore, the proposed mechanism of chain branching of PLA by PGE was illustrated in Fig. 1, which involved epoxide ring-opening reactions and the creation of covalent bonds via hydroxyl side group formation. Moreover, due to the low thermal stability of PLA, the reaction system represented a complex set of degradation and chain branching balance.

^{13}C NMR was used to confirm the structure of the chain branched PLA. Figure 1 depicted the ^{13}C NMR spectrum of PLA and chain branched PLA in $CDCl_3$. It can be seen that three identifiable peaks can be observed for PLA before chain branching. The peak at δ16.62 ppm was assigned to methyl carbons (a-CH_3) of PLA. The peak at δ68.99 ppm belonged to the methine carbon (c-CH-) and the resonance centered at δ169.58 ppm was the typical chemical shifts for ester group carbon (b-COO-). After chain branching, three new resonances can be observed at δ57.22ppm, δ72.72ppm and δ127.55ppm corresponding to

methylene (d-CH_2- and e-CH_2-) and methine carbon (f-CH-) of PGE units, respectively. Because the amount of methyl carbons (a-CH_3) on PLA chain maintained constant before and after chain branching, it can be used as internal standard peak. Compared with the intensity of the internal standard peak, the signal intensity for ester group carbon at δ169.58 increased after chain branching, which together with the appearances of the three new resonances indicated that chain branching reaction occurred between epoxide groups and terminal carboxyl groups.

Dynamic rheological frequency sweeps were used to determine differences in the entanglement structure for neat and chain branched PLA. Fig. 2(a) showed the complex viscosity (η*) as a function of frequency. It was found that curves for both PLA and chain branched PLA exhibited typical Newtonian behavior at low frequency and shear thinning behavior at higher frequency. However, all chain branched samples exhibited higher complex viscosities than neat PLA at full frequency range, and the transition of the complex viscosity curves from Newtonian-plateau to shear thinning regime was shifted to lower frequency indicating the enhanced entanglement between PLA molecules. With increasing PGE content, the complex viscosities initially increased and then declined above 0.5wt% of PGE due to the plasticizing effect of the unreacted PGE.

The Cross equation [23] can be applied to investigate the effect of chain branching on the rheological parameters of PLA, which is written as

$$\eta^*_{(\omega)} = \frac{\eta_0}{1 + (\lambda\omega)^n} \qquad (2)$$

where $\eta^*_{(\omega)}$ is the complex viscosity, ω is the frequency, η_0 is the Newtonian viscosity, λ is a relaxation time whose reciprocal accounts for the onset of shear-thinning region and n is a shear-thinning index.

By fitting the experimental data into the Cross equation, rheological parameter η_0 can be obtained as listed in Tab.1. It can be seen that η_0 initially increased steadily with the increase in PGE content from 0.1 to 0.5wt%, however, it later on decreased somewhat with further rise in content of PGE. Since the chain branched samples can be considered as a mixture of original and chain branched components, the zero-shear viscosities of samples after chain branching were assumed to follow a logarithmic mixing rule [24]:

$$\eta_{0,BL} = \eta_{0,L}^{1-x}\eta_{0,B}^{x} \qquad (3)$$

where, $\eta_{0,BL}$ is the zero-shear viscosity of chain branched PLA; $\eta_{0,L}$ is the zero-shear viscosity of PLA before chain branching; $\eta_{0,B}$ is the zero-shear viscosity of 100% chain branched PLA; x is branching degree.

Following Graessley's review analyzing the up to then experimental evidence on the viscoelastic behavior in the presence of branches [25], and de Gennes' introduction of path fluctuations as the mechanism of the conformational renewal of long tethered chains [26], it has been proved that the zero-shear viscosity ($\eta_{0,B}$) of entangled chain branched molecules, varies (in essence) exponentially with the molecular weight of each of the protruding arms [27]:

$$\frac{\eta_{0,B}}{\eta_{0,BL}} = \sqrt{\frac{M_L}{M_{BL}}}\exp\left\{\alpha\left(\frac{M_L}{M_C} - 1\right)\right\} \qquad (4)$$

where, M_L is the molecular weight of PLA before chain branching, M_L=10,000g/mol here obtained from GPC; M_{BL} is the molecular weight of modified PLA; M_C is the molecular weight at the onset of entanglements, M_c=9,900g/mol according to the references.

By comparing Eqs.3 and 4, an expression for estimating the degree of branching may then be derived:

$$x \approx \frac{\ln\left(\eta_{BL}/\eta_{L}\right)}{\alpha\left(\frac{M_L}{M_e} - 1\right) - 3\ln\left(\frac{M_L}{M_e}\right) + 3.5\ln 2} \qquad (5)$$

where, $Mc/2 = Me$.

The branching degree for PLA chain branched with 0~1wt% PGE can be easily obtained from Eq.5, as listed in Tab.1. When PGE content increased from 0.1wt%PGE to 0.5wt%PGE, the branching degree increased quickly from 0 to 12.69mol%, however, it later on decreased somewhat with further rise in content of PGE, indicating that appropriate PGE content was favored to chain branching reaction.

The tanδ curves of PLA were shown in Fig. 2(b). For neat PLA, tanδ decreased continuously with the frequency, and no plateau of the tanδ curve can be observed, which exhibited a typical terminal behavior of liquid-like material. For samples after chain branching, tanδ decreased quickly at low frequency and then showed a plateau in the frequency range of 10~100Hz. The fact that tanδ is independent of the frequency in a limited frequency range suggested gel-like rheological behavior of PLA due to the existence of long branched chain.

The elastic modulus (G') and viscous modulus (G") of all samples plotted as a function of frequency was shown in Fig.2(c) and (d). It can be seen that G' and G" were both enhanced after chain branching, and the values reached maximum at 0.5wt% PGE content which indicating the enhanced molecular entanglement between PLA chains.

It is known that the melt elasticity and viscosity have a direct relationship with the melt strength which is an indication of the resistance for a melt to extension. Accordingly, the observed improvement in viscous and elastic properties for chain branched PLA encouraged us to perform solid hot drawing processing on them and high draw ratio can be reached by

chain branching. The maximum draw ratio of chain branched PLA with 0.5wt% PGE was 200% higher than that of neat PLA.

3.2 Orientation structure and properties of drawn PLA

3.2.1 Orientation and crystallization properties

The XRD patterns of the PLA and chain branched PLA/0.5wt%PGE before and after drawing were shown in Fig.3(A). The isotropic sample did not show any Debye-Scherrer diffraction rings due to its low crystallinity and the random arrangement of grains. While for the samples oriented, the (200)/(110) reflection appeared as two strong circular spots on the equator and (203) reflection formed a four-point image. With increasing draw ratio, these arcs became narrower in spread and more prominent, suggesting that the crystal axis was preferentially oriented perpendicular to the draw direction.

The corresponding azimuth integrated intensity curves were shown in Fig.3(B). There were two diffraction peaks for oriented PLA at $2\theta \approx 16.7^{o}$ and 18.3^{o}, which could be assigned to the crystal planes (200)/(110) and (203) of α or α' crystal forms of PLA, respectively. Previous studies had shown that PLA can form a disordered α crystalline form (α') where chain conformation and chain-packing are different as compared to the ordered α crystal form with additional diffraction peaks at $2\theta \approx 14.5^{o}$ and 22.2^{o} [28]. Therefore, the crystal structure of oriented PLA in this study can be attributed to α' crystalline form. It can be seen that the diffraction peak position of oriented PLA with different draw ratio had no change, however, there were significant differences in intensity, indicating that drawing significantly affected the crystallization and orientation of PLA.

The crystallinity of PLA and chain branched PLA can be calculated by the peak area of crystal and amorphous region from the corresponding decomposed curves obtained by PeakFit software. The orientation parameter (f) was calculated using Herman's orientation function:

$$f = \frac{3\left\langle \cos^2 f \right\rangle - 1}{2} \quad (7)$$

$$\left\langle \cos^2 \phi \right\rangle = \frac{\int_0^{\pi/2} I(\phi) \sin\phi \cos^2\phi \, d\phi}{\int_0^{\pi/2} I(\phi) \sin\phi \, d\phi} \quad (8)$$

Where I(ϕ) is the scattering intensity along the angle ϕ. When taking ϕ = 0 as the shear flow direction, the critical values of fare −0.5 for a perfect perpendicular orientation, 0 for a random orientation and 1 for a perfect parallel orientation, respectively.

The crystallinity and orientation factor were summarized in Fig.3(C). With the increase of draw ratio, the crystallinity and orientation factor of PLA increased, indicating that slipping and rupture of the lamellar in the spherulite occurred during the drawing of PLA and a clear orientation of PLA molecules formed.

3.2.2 Mechanical Properties

The mechanical properties of PLA and chain branched PLA/0.5wt%PGE with varing draw ratio were shown in Fig.4. Before orientation, compared to the neat PLA, chain branching did not bring about remarkable change in tensile strength and modulus. With increasing drawing ratio, the tensile strength and modulus increased sharply, while the elongation at break decreased for both neat PLA and chain branched PLA. At 800% of drawing ratio, the tensile strength of chain branched PLA reached up to 105±5 MPa, and the tensile modulus was 4.1±0.2GPa.

3.3 Blood Compatibility of Oriented PLA

When platelets are activated, they will deform and crosslink to promote aggregation of further platelets. Platelet adhesion and activation on the surface of a biomaterial is the most essential character in determining the blood compatibility of a biomaterial. Low platelet adhesion and activation denotes good blood compatibility, while a higher degree of platelet adhesion and activation could result in a thrombus.

The platelet adhesion densities on the samples were evaluated, as shown in Fig.5. After contact with PRP for 60 min, a large number of platelets were observed to aggregate on the surface of isotropic PLA. In the case of chain branched PLA/0.5wt%PGE, however, the surface seemed prone to prevent platelets from adhering, since much fewer platelets were observed, indicating that the activation of platelets on chain branched sample was limited. With increasing draw ratio, platelet adherent density on chain branched PLA was further decreased. In addition, platelets on such oriented samples remained their original shape indicating that activation of the intrinsic blood coagulation system was suppressed.

The interactions between plasma proteins and blood-contacting materials strongly affect the thrombotic reaction induced by intrinsic surface contact pathway [29]. What's more, nonspecific adsorption of proteins such as fibrinogen and clotting enzymes on biomaterial surfaces is recognized as the first interaction event of many undesired bio-reactions and bio-responses, followed which were platelet adhesion and activation of coagulation pathways, and then leading to thrombus formation [30]. Two kinds of proteins, bovine serum albumin (BSA) and bovine serum fibrinogen (BFG), were used as the model protein to test the protein adsorption on the surfaces of neat PLA and chain branched PLA/0.5wt%PGE under the static state. As shown in Fig.6 (A) the chain branched PLA had lower BSA and BFG adsorption than those of the neat PLA, and the amount of the adsorbed BSA and BFG decreased further with the increase of draw ratios. The improved protein-resistant properties indicated the enhancement of the blood compatibility of the modified PLA.

The APTT (activated partial thromboplastin time) and TT (thrombin time) tests are widely used for the clinical detection of the abnormality of blood plasma and the primary screening of the anticoagulative chemicals and they are recently applied in the evaluation of the in vitro antithrombogenicity of biomaterials. In general, APTT was used to measure the inhibited efficacy of both the intrinsic (or referred to as the contact activation pathway) and

the common plasma coagulation pathways including factors II, V, X, XII or fibrinogen [31]. TT was used to measure the clot formation time for the thrombin converted fibrinogen into fibrin in the platelet-poor plasma (PPP). The shorter clotting time indicates the faster conversion of fibrinogen to insoluble fibrin protein, which then leads to thrombus [32]. Fig.6 (B) showed APTT and TT of neat PLA and chain branched PLA/0.5wt%PGE. For the APTT tests, the blood clotting time of PLA (39.1 ± 1.3 s) increased compared with the control (37.5 ± 1.1 s), and compared with the neat PLA before drawing, the APTTs of the chain branched PLA (47.6 ± 1.3 s) were longer, which increased further with the increase of draw ratio. The values of TT also increased slightly after chain branching and stretching.

Hemolysis of the blood is an extremely serious problem associated with the bio-incompatibility of materials. Red blood cells may hemolyze when contacting with implant materials and thus cause eventually failure [34]. Therefore, for evaluating blood compatibility and biocompatibility, it is of vital importance to investigate the hemolysis ratio of the material. Results obtained from hemolysis test of acid citrate dextrose anticoagulant blood (ACD) for neat PLA and chain branched PLA/0.5wt%PGE were shown in Fig.6 (C). According to the related standard (ASTM F 756-00), permissible hemolysis ratio of biomaterials should be at least lower than 5%. Therefore, first, the hemolysis ratio of 2.03±0.1% for neat PLA makes it suitable as the substrate material. As to the surface of chain branched PLA before drawing, an obviously less hemolysis rate was obtained indicating that the chain branching would improve the compatibility of the PLA when contacting with biofluids. Sample after drawing with different draw ratio was much less hemolytic than the isotropic one. Therefore, due to less damage of red blood cells, the oriented PLA exhibited desirable blood compatibility.

3.4 Bionic character of oriented PLA

From the material science point of view, a native blood vessel is the best blood compatible material. The intimal layer of the blood vessel can resist platelet adhesion and

prevent undesirable thrombus formation [35]. SEM and AFM images of the blood vessel (Fig.7 (a-b)) showed that the inner surface of the aortic intima was not flat but rather rough at the scale of several microns, with fibrillar structure and micro-grooves. This micro topography of the blood vessel was believed to play an important role in blood compatibility, because this kind of structure led to hydrophobicity of surface and a low chance for contact with platelets.

The cross section and surface morphology of chain branched PLA before orientation were shown in Fig.7 (c) and (d). It can be seen that the cross section and surface architectures of chain branched PLA were smooth and flat. The cross section morphology of the sample with the draw ratio of 800% was shown in Fig.7 (e), which showed concave fibrous structure with regular arranged fibrillar bundle. These micro-fibers were mainly composed of highly oriented folded lamellar crystals and noncrystal parts oriented along the drawing direction which alternately and periodically arranged. The surface morphology of chain branched PLA with the draw ratio of 800% was shown in Fig.7 (f). Surfaces with alternating parallel grooves and ridges at the sub-micron scale can be observed. The average width of the ridges was about 500nm and the height was about 100 nm. Moreover, the water contact angle of PLA increased from 65^{o} before orientation to 112^{o} for the oriented sample, as shown in Fig. 7 (c) and (e), indicating that the hydrophobicity was enhanced after orientation. Therefore, for oriented PLA, it was thought that the different blood compatibility may be due to their different surface morphology and surface properties.

The morphology of oriented PLA was observed to be similar to that of the inner surface of blood vessels. When the surface roughness was within the range of 50 nm (dimension of proteins) to 2 μm (dimension of platelets), particular surface topographies, such as grooves, may reduce the contact area for platelets, which can only adhere on the top of the topographic features; platelet adhesion and thrombus formation may thus be reduced [36].

4. Conclusions

Highly-oriented chain branched PLA with enhanced mechanical properties and good blood compatibility were fabricated through solid hot drawing technology. ^{13}C NMR was used to confirm the structure of the chain branched PLA, indicating that chain branching reaction occurred between epoxide groups and terminal carboxyl groups. It was found that branched degree as high as 12.69 mol% can be obtained after chain branching at 0.5wt% PGE content. The complex viscosity, elastic and viscous modulus as well as molecular entanglement were enhanced by chain branching and higher draw ratio can be achieved. The tensile strength and modulus of samples increased significantly by stretching. The results of in vitro blood compatibility showed that, compared with neat PLA, oriented samples after chain branching exhibited less platelet adhesion, BSA and BFG protein adsorption, longer APTT and TT clotting time, lower hemolysis ratio, indicating that the samples with highly molecular orientation exhibited an appreciably better blood compatibility than neat PLA. Fibrous structure as well as submicrometer structures including alternating parallel grooves and ridges at the micron scale which were similar to intimal layer of blood vessel can be observed for the oriented PLA, and this structure was considered beneficial to decrease the activation and/or adhesion of platelets.

Acknowledgements

This research was supported by National Natural Science Foundation of China (Grant No. 51303109) and International Scientific and Technological Cooperation Project of Sichuan Province (Grant No. 2015HH0019).

References

[1] B.D. Ratner, S.J. Bryant, BIOMATERIALS: Where We Have Been and Where We are Going, Annual Review of Biomedical Engineering, 6 (2004) 41-75.

[2] K. Rezwan, Q.Z. Chen, J.J. Blaker, A.R. Boccaccini, Biodegradable and bioactive porous

polymer/inorganic composite scaffolds for bone tissue engineering, Biomaterials, 27 (2006) 3413-3431.

[3] W.Y. Yeong, C.K. Chua, K.F. Leong, M. Chandrasekaran, Rapid prototyping in tissue engineering: challenges and potential, Trends in Biotechnology, 22 (2004) 643-652.

[4] J.W. Xie, M.R. MacEwan, W.Z. Ray, W. Liu, D.Y. Siewe, Y.N. Xia, Radially Aligned, Electrospun Nanofibers as Dural Substitutes for Wound Closure and Tissue Regeneration Applications, ACS Nano, 4 (2010) 5027-5036.

[5] W.K. Czaja, D.J. Young, M. Kawecki, R.M. Brown, The Future Prospects of Microbial Cellulose in Biomedical Applications, Biomacromolecules, 8 (2007) 1-12.

[6] S.L. Bourke, J. Kohn, Polymers derived from the amino acid l-tyrosine: polycarbonates, polyarylates and copolymers with poly(ethylene glycol), Advanced Drug Delivery Reviews, 55 (2003) 447-466.

[7] J.F. Mano, R.A. Sousa, L.F. Boesel, N.M. Neves, R.L. Reis, Bioinert, biodegradable and injectable polymeric matrix composites for hard tissue replacement: state of the art and recent developments, Composites Science and Technology, 64 (2004) 789-817.

[8] P. Gunatillake, R. Mayadunne, R. Adhikari, Recent developments in biodegradable synthetic polymers, Biotechnology Annual Review, 12 (2006) 301-347.

[9] R Noriega, J Rivnay, K Vandewal, FPV Koch, A general relationship between disorder, aggregation and charge transport in conjugated polymers , Nature materials, 12 (2013) 1038-1044.

[10] M Mas-Torrent, C Rovira, C. Role of molecular order and solid-state structure in organic field-effect transistors. Chem. Rev. 111 (2011) 4833-4856.

[11] Z Li, X Zhao, L Ye, P Coates, F Caton-Rose, M Martyn, Structure and blood compatibility of highly oriented poly (l-lactic acid) chain extended by ethylene glycol diglycidyl ether, Polymer, 56 (2015) 523-534.

[12] Z.Q. Li, X.W. Zhao, L. Ye, P. Coates, F.C. Rose, M. Martyn, Structure and blood compatibility of highly oriented PLA/MWNTs composites produced by solid hot drawing, J Biomater Appl, 28 (2014) 978-989.

[13] D.W. Grijpma, H. Altpeter, M.J. Bevis, Improvement of the mechanical properties of poly (D, L‐lactide) by orientation, Polymer international, 51 (2002) 845-851.

[14] F. Yang, X. Qu, W. Cui, J. Bei, F. Yu, S. Lu, S. Wang, Manufacturing and morphology structure of polylactide-type microtubules orientation-structuredscaffolds, Biomaterials, 27 (2006) 4923-4933.

[15] L Wang, RL Shogren, C Carriere, Preparation and properties of thermoplastic starch-polyester laminate sheets by coextrusion, Polymer Engineering & Science, Volume 40 (2000) 499-506.

[16] G. Stoclet, R. Seguela, J.M. Lefebvre, S. Elkoun, C. Vanmansart, Strain-Induced Molecular Ordering in Polylactide upon Uniaxial Stretching, Macromolecules, 43 (2010) 1488-1498.

[17] K. Hiltunen, M. Härkönen, J.V. Seppälä, T. Väänänen, Synthesis and Characterization of Lactic Acid Based Telechelic Prepolymers, Macromolecules, 29 (1996) 8677-8682.

[18] J. Kylmä, J. Tuominen, A. Helminen, J. Seppälä, Chain extending of lactic acid oligomers. Effect of 2,2’-bis(2-oxazoline) on 1,6-hexamethylene diisocyanate linking reaction, Polymer, 42 (2001) 3333-3343.

[19] C.Wendeln, B.J. Ravoo, Surface Patterning by Microcontact Chemistry, Langmuir, 28 (2012), 5527-5538.

[20] M.D. Bentley, X. Zhao, X. Shen, W.D. Battle, Branched Polymers, US Patent App. 13/865, 912, 2013.

[21] N. Orakdogen, B.Erman, O. Okay, Evidence of Strain Hardening in DNA Gels, Macromolecules, 43 (2010), 1530-1538.

[22] D. Costa, J. Queiroz, M.G. Miguel, B. Lindman, Swelling behavior of a new biocompatible plasmid DNA hydrogel, Colloids and Surfaces B: Biointerfaces, 92 (2012) 106-112.

[23] A. A. Haralabakopoulos, D. Tsiourvas, C.M. Paleos, Chain extension of poly(ethylene terephthalate) by reactive blending using diepoxides, Journal of Applied Polymer Science, 71 (1999) 2121-2127.

[24] L. Incarnato, P. Scarfato, L.D. Maio, D. Acierno, Structure and rheology of recycled PET modified by reactive extrusion, Polymer, 41 (2000) 6825-6831.

[25] S. Japon, L. Boogh, Y. Leterrier, J.A.E. Månson, Reactive processing of poly(ethylene terephthalate) modified with multifunctional epoxy-based additives, Polymer, 41 (2000) 5809-5818

[26] C. Decker, T.N. ThiViet, D. Decker, E.W. Koehl, UV-radiation curing of acrylate/epoxide systems, Polymer, 42 (2001) 5531-5541.

[27] K. Lamnawar, A. Maazouz, Rheological study of multilayer functionalized polymers: characterization of interdiffusion and reaction at polymer/polymer interface, Rheologica acta, 45 (2006) 411-424.

[28] S.A. Madbouly, J.U. Otaigbe, A.K. Nanda, D.A. Wicks, Rheological Behavior of Aqueous Polyurethane Dispersions: Effects of Solid Content, Degree of Neutralization, Chain Extension, and Temperature, Macromolecules, 38 (2005) 4014-4023.

[29] J. Liu, L. Lou, W. Yu, R. Liao, R. Li, C. Zhou, Long chain branching polylactide: Structures and properties, Polymer, 51 (2010) 5186-5197.

[30] K. Wasanasuk, K. Tashiro, M. Hanesaka, T. Ohhara, Crystal Structure Analysis of Poly (l-lactic Acid) α Form On the basis of the 2-Dimensional Wide-Angle Synchrotron X-ray and Neutron Diffraction Measurements, Macromolecules, 44 (2011), 6441-6452.

[31] L. L. K. Leung, ASH Education Program Book, 2006, 457-461.

[32] M.M. Flanders, R. Crist, G.M. Rodgers, Comparison of five thrombin time reagents, Clin. Chem., 49 (2003), 169-172.

[33] S. Agathopoulos, P. Nikolopoulos, Wettability and interfacial interactions in bioceramic body liquid system, J Biomed Mater Res, 29 (1995) 421-429.

[34] H. Fan, P. Chen, R. Qi, J. Zhai, D. Han, L. Jiang, Greatly Improved Blood Compatibility by Microscopic Multiscale Design of Surface Architectures, Small, 19 (2009) 2144-2148.

[35] A.D. Mel, G. Jell, M.M. Stevens, A.M. Seifalian, Biofunctionalization of Biomaterials for Accelerated in Situ Endothelialization: A Review, Biomacromolecules, 9 (2008) 2969-2979.

[36] L. Chen, D. Han, L. Jiang, On improving blood compatibility: From bioinspired to synthetic design and fabrication of biointerfacial topography at micro/nano scales, Colloids and Surfaces B: Biointerfaces, 85 (2011) 2-7.

Table caption

Tab. 1. Rheological parameters and maximum draw ratio of PLA

Figure captions

Fig. 1. (a): Proposed reaction between PLA and PGE; (b): ^{13}C NMR spectrum (600MHz, $CDCl_3$) for PLA.

Fig.2. (a): Complex viscosity vs frequency for PLA and PLA/PGE at 170°C; (b): Tanδ vs frequency for PLA and PLA/PGE at 170°C; (c): Elastic modulus vs frequency for PLA and PLA/PGE at 170°C; (d): Viscous modulus vs frequency for PLA and PLA/PGE at 170°C.

Fig.3. (A): Two-dimensional XRD patterns of oriented PLA and PLA/0.5wt%PGE with different draw ratio; (B): XRD curves of PLA and PLA/0.5wt%PGE with different draw ratio; (C): Orientation factor and crystallinity of PLA and PLA/0.5wt%PGE with different draw ratio. (Values are expressed as means ± SD, n = 3).

Fig.4. Mechanical properties of PLA and PLA/0.5wt%PGE with varying draw ratio (Values are expressed as means ± SD, n = 5).

Fig.5. Platelet adsorption of PLA and PLA/0.5wt%PGE with different draw ratio (Magnification: 5000×) (Values are expressed as means ± SD, n = 3).

Fig.6. (A): BSA and BFG adsorptions on the oriented PLA and PLA/0.5wt%PGE; (B): clotting time of oriented PLA and PLA/0.5wt%PGE; (C): hematolysis ratio of oriented PLA and PLA/0.5wt%PGE (Values are expressed as means ± SD, n = 3).

Fig.7. (a,b): Blood vessel structure; (c,d): The structure of PLA/0.5wt%PGE before orientation; (e,f): The structure of PLA/0.5wt%PGE after orientation; Upper-left corner of (d) and (f): The water contact angle for PLA/0.5wt%PGE before and after orientation.

Table

Table 1 Rheological parameters and maximum draw ratio of PLA

Parameters	PLA	PLA/0.1wt %PGE	PLA/0.3wt % PGE	PLA/0.5wt % PGE	PLA/0.7wt % PGE	PLA/1wt% PGE
$\eta_{0,BL}$ ($10^{\wedge 3}$ Pa.s)	0.539	0.806	1.012	1.302	1.267	1.158
Branching degree (mol%)	0	5.96	9.64	12.69	11.35	10.99
Maximum draw ratio (%)	600	600	700	800	700	500

Figures

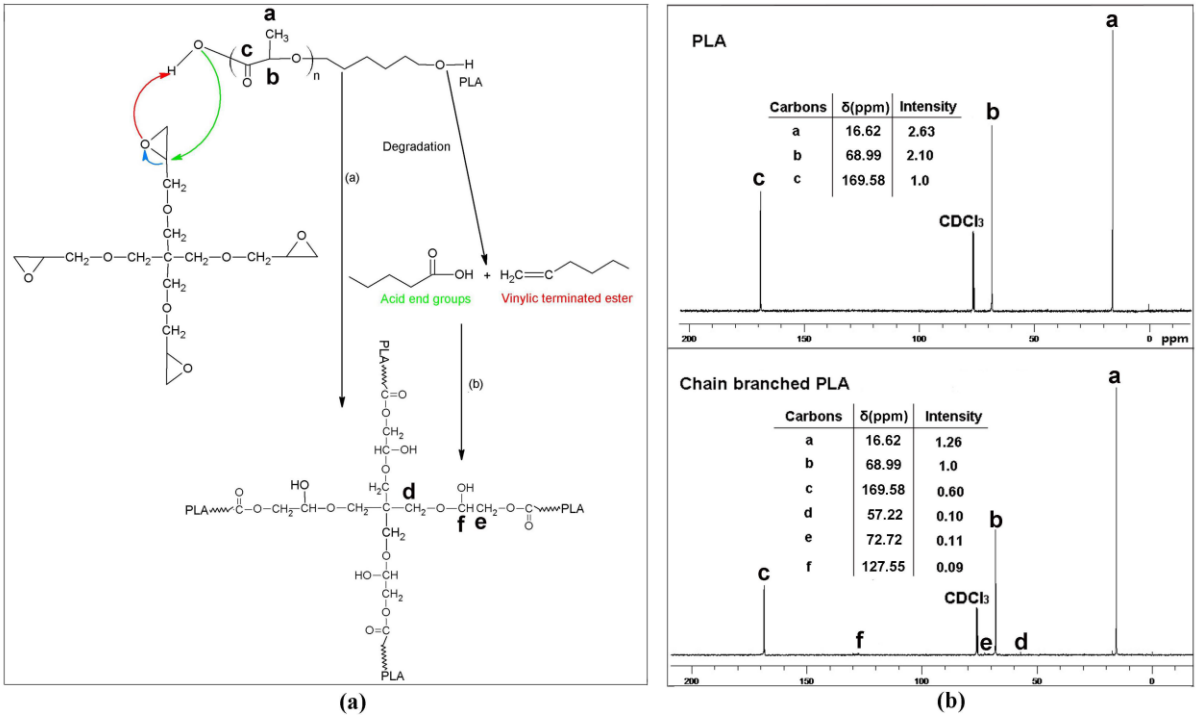

(a) (b)

Fig. 1. (a): Proposed reaction between PLA and PGE; **(b)**: ^{13}C NMR spectrum (600MHz, CDCl3) for PLA.

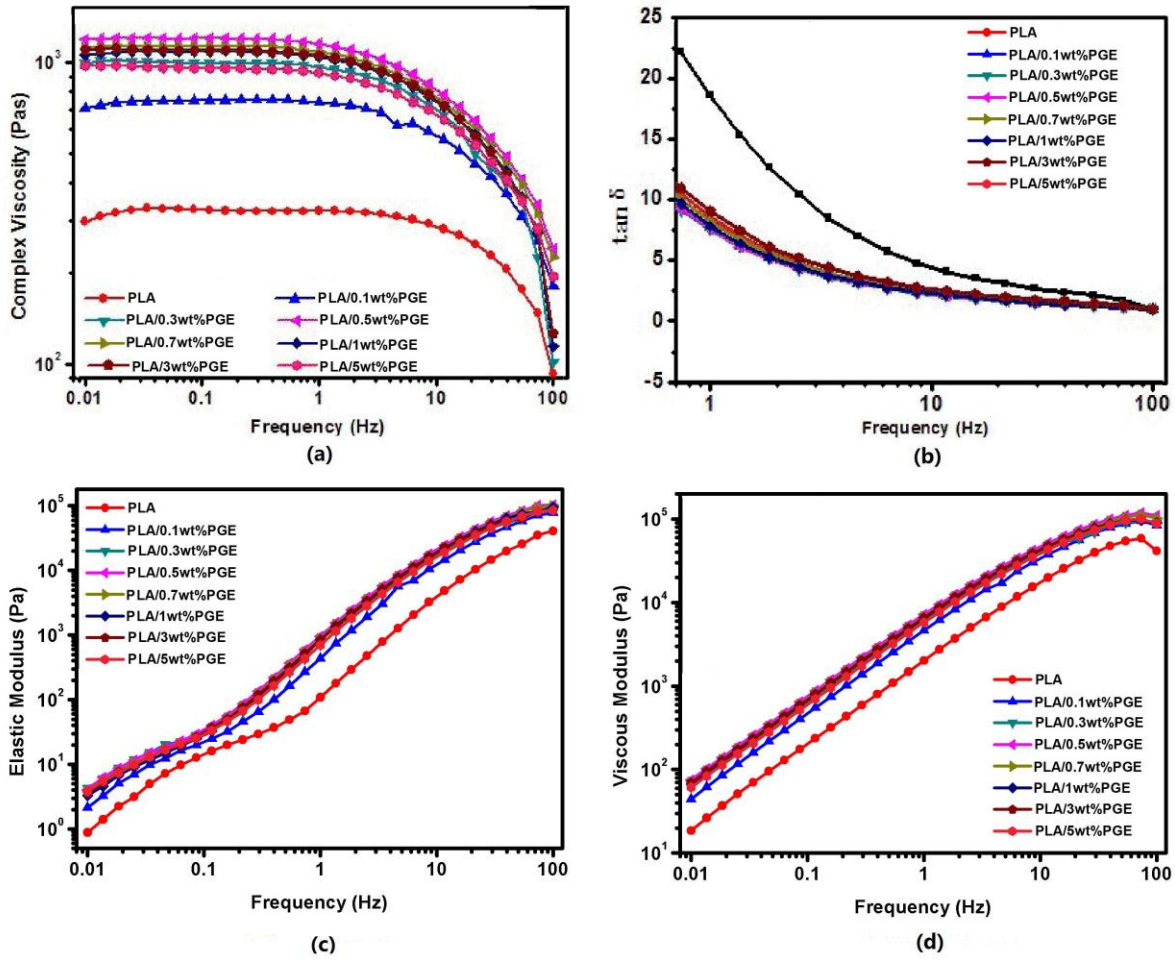

Fig.2. (a): Complex viscosity vs frequency for PLA and PLA/PGE at 170°C; (b): Tanδ vs frequency for PLA and PLA/PGE at 170°C; (c): Elastic modulus vs frequency for PLA and PLA/PGE at 170°C; (d): Viscous modulus vs frequency for PLA and PLA/PGE at 170°C.

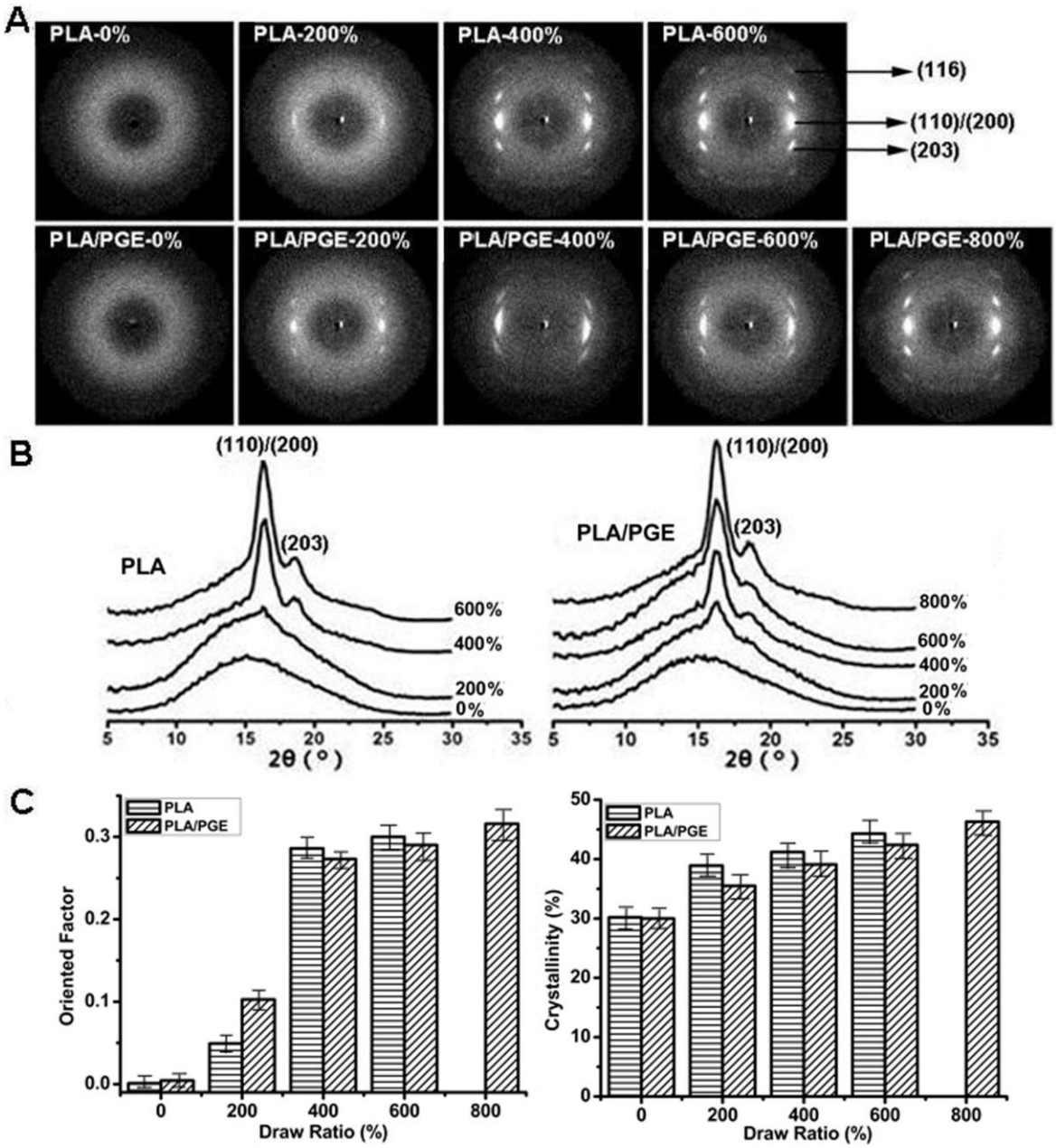

Fig.3. (A): Two-dimensional XRD patterns of oriented PLA and PLA/0.5wt%PGE with different draw ratio; (B): XRD curves of PLA and PLA/0.5wt%PGE with different draw ratio; (C): Orientation factor and crystallinity of PLA and PLA/0.5wt%PGE with different draw ratio. (Values are expressed as means ± SD, n = 3).

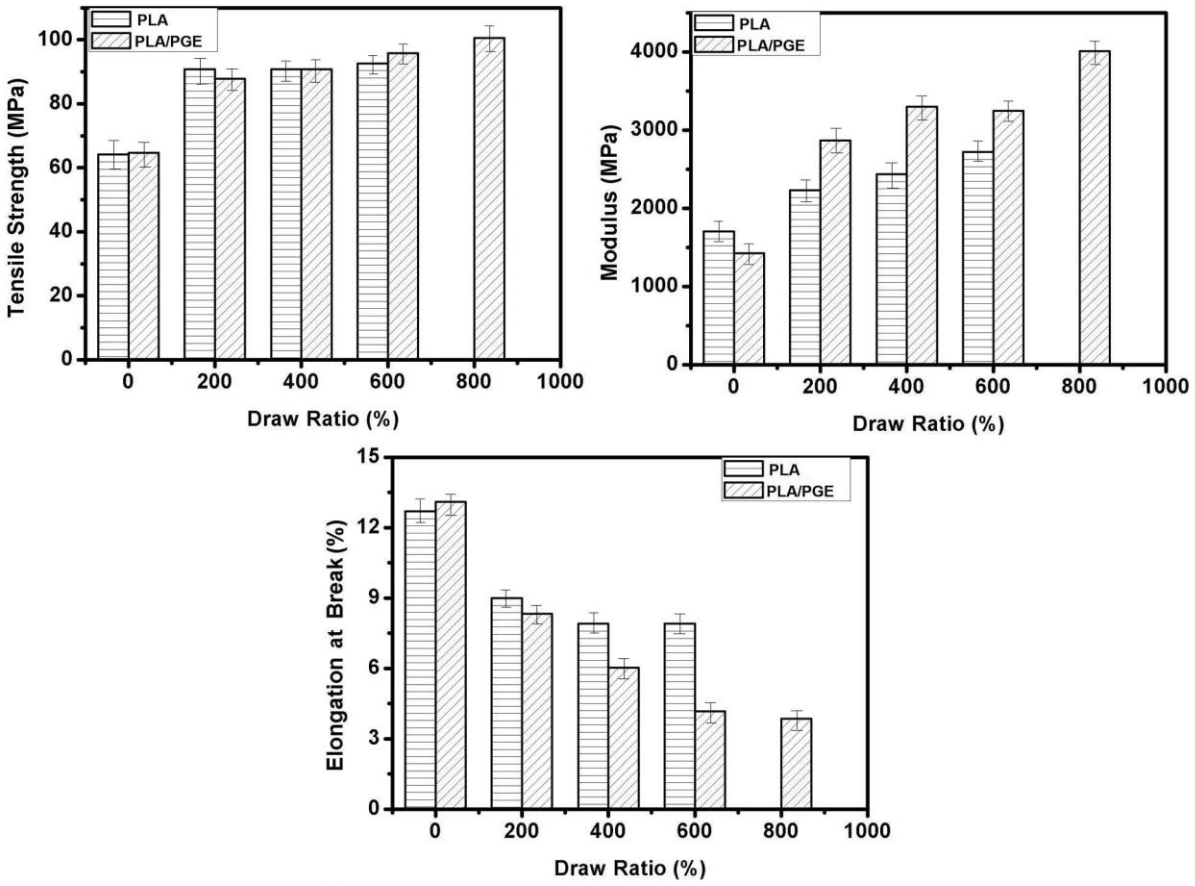

Fig.4. Mechanical properties of PLA and PLA/0.5wt%PGE with varying draw ratio (Values are expressed as means ± SD, n = 5).

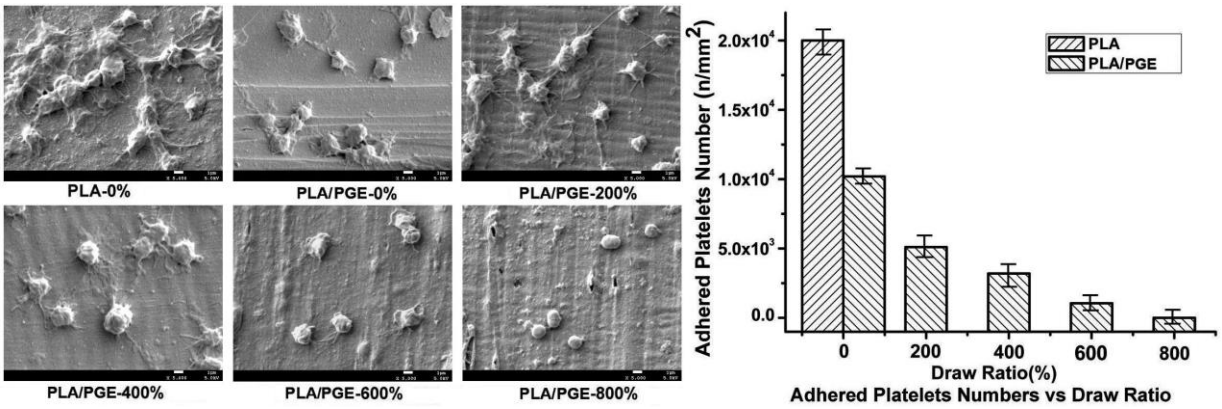

Fig.5. Platelet adsorption of PLA and PLA/0.5wt%PGE with different draw ratio (Magnification: 5000×) (Values are expressed as means ± SD, n = 3).

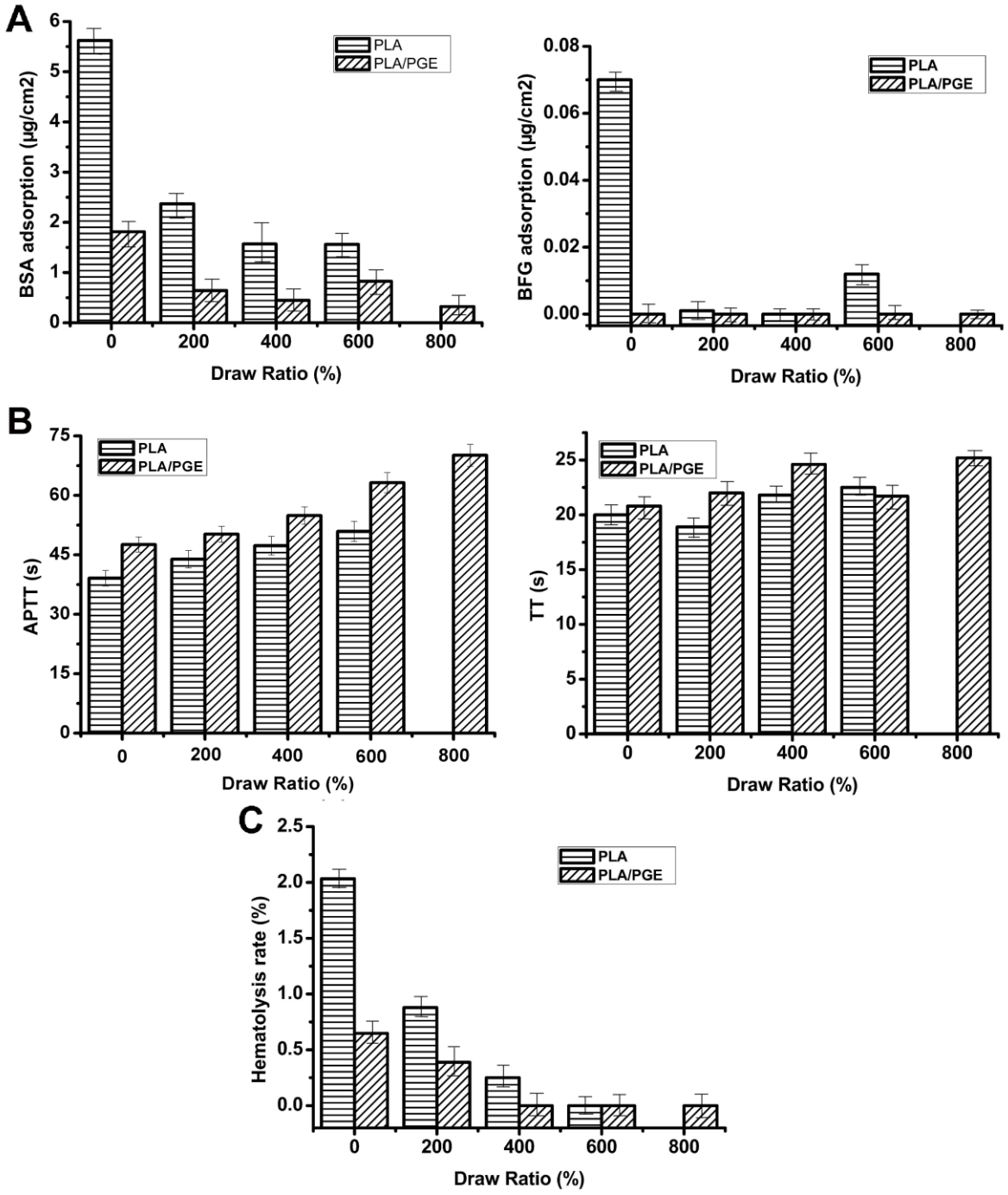

Fig.6. (A): BSA and BFG adsorptions on the oriented PLA and PLA/0.5wt%PGE; (B): clotting time of oriented PLA and PLA/0.5wt%PGE; (C): hematolysis ratio of oriented PLA and PLA/0.5wt%PGE (Values are expressed as means ± SD, n = 3).

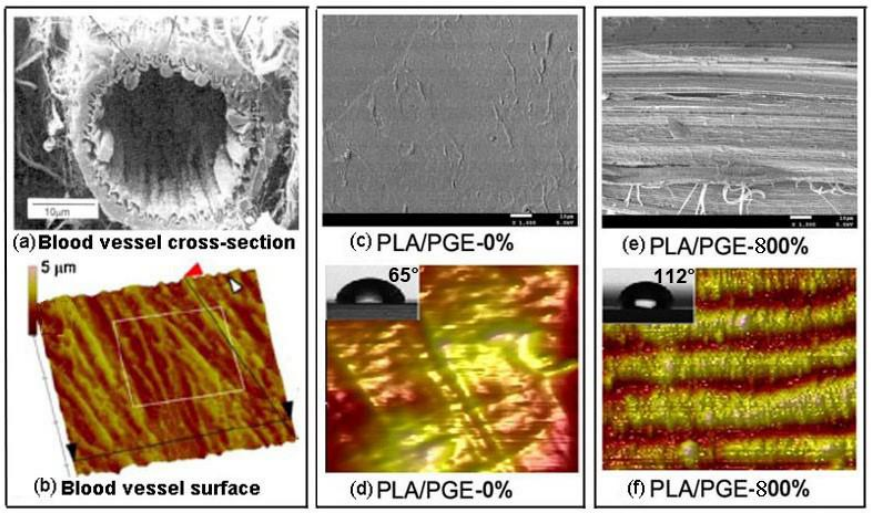

Fig.7. (a,b): Blood vessel structure; (c,d): The structure of PLA/0.5wt%PGE before orientation; (e,f): The structure of PLA/0.5wt%PGE after orientation; Upper-left corner of (d) and (f): The water contact angle for PLA/0.5wt%PGE before and after orientation.